

Investigation of Calcium–Aluminate-Based Mold Flux of Different Compositions

Irmtraud Marschall* and Harald Harmuth

The liquidus temperature, crystallization behavior, and viscosity of calcium–aluminate (CA)-based mold flux systems are investigated by differential thermal analysis, quench tests, and viscosity measurements to understand the impact of SrO, B₂O₃, F, and Li₂O on the flux properties. For mixtures with a CaO/Al₂O₃ (wt%) ratio of 1, the liquidus temperature of 1443 K and a viscosity of 0.37 Pa s are achieved with the addition of 6.5 wt% B₂O₃. Substitution of CaO for 8.3 wt% SrO in the B₂O₃-free compositions increases a liquidus temperature from 1547 to 1559 K, and 2.6 wt% increases the viscosity from 0.35 to 0.41 Pa s, indicating that low amount SrO is not beneficial in adjusting slag properties of CA mold flux. A fluorine content of up to 6.1 wt% decreases the melting temperature from 1547 to 1509 K and inhibits crystallization while promoting volatilization in the liquid state. Li₂O (2.3 wt%) effectively enhances the glass-forming ability of the CA mold flux and decreases both the liquidus temperature from 1571 to 1509 K and the viscosity of the system from 0.43 to 0.28 Pa s. This study deepens the knowledge on CA flux systems, which could be useful for their effective design.

1. Introduction

During a continuous casting process, Al from steel reacts with SiO₂ from the mold flux to form Al₂O₃ and Si,^[1–3] altering the chemical composition of the mold flux and, consequently, its properties. In particular, when casting Al-alloyed steel grades, modifying the slag composition increases their viscosity, liquidus temperature, and crystalline fraction.^[1,2,4] Therefore, less reactive CaO–Al₂O₃ (CA)-based mold fluxes with lower SiO₂ contents (<10 wt%) have been developed.^[5–8] However, lubrication, crystallization, and heat transfer issues still persist. Contrary to the silicate structure of CaO–SiO₂-based mold fluxes, the structure of

CA-based mold fluxes consists mainly of aluminate structural units with three coordination numbers—^{IV}Al, ^VAl, and ^{VI}Al, of which only ^{IV}Al participates in the formation of a network structure.^[9] In addition, the initial crystallization of CA-based mold flux is higher than that of CaO–SiO₂-based mold flux, and their crystallization mechanism consequently differs.^[10,11] In contrast to CaO–SiO₂-based mold flux, as the cooling rate of CA-based flux increases from 5 to 50 K min^{−1}, their phases and crystal morphologies remain the same.^[11] As the morphology and quantity of crystals precipitated from mold slag greatly affect the formation of the slag rim, improving lubrication and the prevention of thick slag rims remain the main challenges in this field.^[8,12,13]

An literature study was conducted to identify the essential constituents of CA-based mold flux systems. The slag viscosity can be altered by adjusting the number of network modifiers. The optimum CaO/Al₂O₃ (wt%, C/A) ratio was found to be between 0.9 and 1.6.^[12,14] The addition of MgO, Li₂O, Na₂O, and TiO₂ and 15–30 wt% SrO decreases the viscosity of CA-based mold flux. The addition of 3–6 wt% BaO as a substitute to CaO increases the viscosity of the flux; however, further increasing BaO from 5 to 20 wt% decreases the viscosity.^[15–19] Moreover, the use of B₂O₃ is noted to be the most effective method to address the issues of CA-based flux systems. B³⁺ mainly forms the [BO₃] structural unit in the CA mold flux system, forming a 2D structure that is less interconnected than a tetrahedron.^[20,21] These changes to simpler structures reduce the viscosity of the system. In contrast to traditional slag systems where fluorine is solely a fluxing agent, fluorine contents exceeding 6.9 wt% do not have any further effect in reducing the viscosity of the CA system.^[22]

To achieve good glass-forming ability and a low liquidus temperature, the crystallization of mold flux systems needs to be controlled. In terms of melting temperature, the optimum C/A ratio in a CA binary in which low melting temperatures can be achieved is in the range of 0.6–1.8.^[7,12] Considering viscosity as a cofactor, this range is narrowed to 1.1–1.6.^[23] However, without additional components, the resulting crystallization temperature remains extremely high. Thus, B₂O₃, Li₂O, BaO, SrO, and TiO₂, and small amounts of CaF₂ have been reported to inhibit crystallization by lowering the starting temperature and prolonging the incubation time.^[18,19,24,25] In contrast, an increase in the crystallization and break temperatures was reported with the increasing contents of Na₂O, TiO₂, MgO, and BaO, and large quantities of CaF₂.^[17,23,25–28] Similarly

Dr. I. Marschall
K1-Met GmbH
Peter Tunner-Straße 5, Leoben 8700, Austria
E-mail: irmtraud.marschall@unileoben.ac.at

Dr. I. Marschall, Prof. H. Harmuth
Chair of Ceramics
Montanuniversitaet Leoben
Peter Tunner-Straße 5, Leoben 8700, Austria

 The ORCID identification number(s) for the author(s) of this article can be found under <https://doi.org/10.1002/srin.202100187>.

© 2021 The Authors. Steel Research International published by Wiley-VCH GmbH. This is an open access article under the terms of the Creative Commons Attribution-NonCommercial License, which permits use, distribution and reproduction in any medium, provided the original work is properly cited and is not used for commercial purposes.

DOI: 10.1002/srin.202100187

to SiO_2 , B_2O_3 , and Na_2O are reduced by the Al from steel.^[8,29] Simultaneously, fluorine partly evaporates, forming LiF, NaF, and SiF_4 .^[30] Although the number of reports focusing on CA-based mold flux systems has increased in the past 7 years, there is still limited data available.

In this study, to achieve their industrial applicability, CA-based mold flux was investigated based on the following requirements: a liquidus temperature of <1523 K, a viscosity of <0.25 Pa s at 1573 K, and high glass-forming ability. The properties of CA-based mold fluxes of different compositions, including sample with and without boron, and small amounts of Li_2O partly replaced by Na_2O , were investigated. Furthermore, the impact of SrO on the slag properties was tested.

2. Experimental Section

Thermochemical calculations were performed using FactSage software (release 7.3, CON3 and FactPS database) to estimate the liquidus temperatures and viscosity at 1573 K of CA-based mold flux with different compositions. To meet the specified requirements, two approaches were considered—compositions with and without B_2O_3 . First, the amounts of SiO_2 and fluorine were restricted to 6 and 3 wt%, respectively. B_2O_3 substituted SiO_2 as the network builder. Second, as B_2O_3 can be reduced by Al from steel similar to SiO_2 , compositions without B_2O_3 were also considered. In this case, the amount of fluorine was not controlled. Based on the FactSage results, appropriate chemical compositions were selected for further investigations. A comparison between the measured and the calculated values is given in Figure 1. It has to be admitted that the phases implemented in FactSage do not meet the phases detected in the experiments. Hence, the liquidus temperature is overestimated by FactSage. The detailed chemical compositions, measured viscosity values at 1573 K, and liquidus and break temperatures are listed in Table 1.

For each composition, analytical grades SiO_2 (Quartz, Roth, $>99.0\%$), Al_2O_3 (Sigma-Aldrich, $>98.0\%$), CaCO_3 (Roth, $\geq 98.5\%$), Na_2CO_3 (Roth, $>99.5\%$), Li_2CO_3 (Roth $>99\%$), CaF_2 (Roth $>99.0\%$), B_2O_3 (Sigma-Aldrich, $>98.0\%$), SrCO_3 (Sigma-Aldrich, $>98.0\%$), MgO (Roth, $>98\%$), K_2CO_3 (Honeywell Fluka, $>99\%$), and TiO_2 (Sigma-Aldrich, $>99.0\%$) were mixed and heated at 973 K for 7 h to partially dissociate the used carbonates. The glass-forming ability of the samples is tested by melting 25 g of the mixtures shown in Table 1 at 1673 K for 15 min within a Pt crucible in a laboratory furnace (HT16/17, Nabertherm) and quenching the mixture to room temperature on a steel plate. The crystalline phase was analyzed by X-ray diffraction (XRD) using a Bruker D8 device with a LYNXEYE detector, copper source, and fixed divergence slit. The measurement time per step was set to 1 s at an interval of 0.01° . The liquidus temperatures were determined using a simultaneous thermal analysis (STA) 449 F3 Jupiter (Netzsch). The temperature was calibrated with standard reference material Sn, Al, Au, and Pd. The balance was checked with calcium oxalate monohydrate. A differential thermal analysis (DTA) sample carrier was used with the sample chamber purged with Ar. The sample (100 mg) was placed in a covered Pt/Ir crucible, heated at 20 K min^{-1} up to 1723 K and cooled down to 576 K at 10 K min^{-1} . The crystallization results of the quenched samples obtained by STA are not representative of the intended

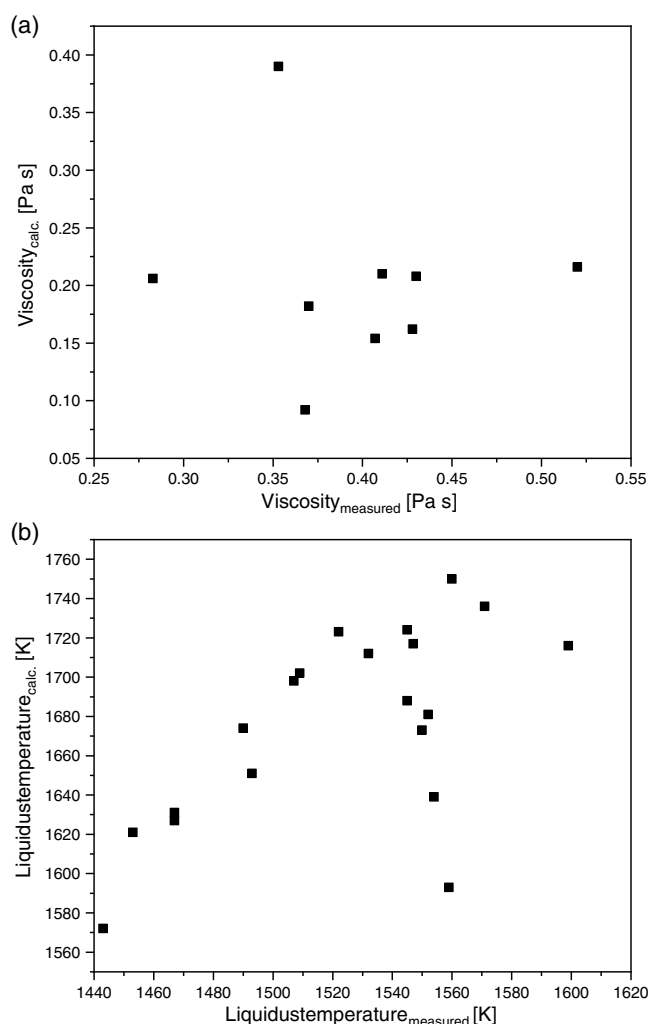


Figure 1. Comparison of calculated and measured values: a) viscosity and b) liquidus temperature.

chemical compositions due to the vaporization of the volatile components and low specimen mass. Therefore, furnace crystallization test (FCT), which represents a macroscale DTA, was performed on samples 0–3 (27 g). The samples and Al_2O_3 , which was used as the reference, were placed in Pt crucibles, respectively, in a laboratory furnace (RHF 16/8, Carbolite), heated at 5 K min^{-1} up to 1673 K and maintained for 15 min, and then cooled down to room temperature at 10 K min^{-1} . The temperature was measured using a type-S thermocouple. For samples 14 and 17–19, the time dependence of the crystallization was investigated using two furnaces (HT16/17, Nabertherm and RHF 16/8, Carbolite). In the Nabertherm furnace, the samples were melted at 1673 K for 15 min in a Pt crucible. The melted sample was then cast into a steel crucible and maintained at 1173 K in the Carbolite furnace for 5, 15, 30, and 60 min. After the FCT and dwell tests, the microstructure of the samples was examined microscopically (scanning electron microscope (SEM): EVO MA 15, Zeiss AG, energy dispersive spectroscopy (EDS): INCA Drycool detector, Oxford Instruments) and by XRD. The viscosity at different temperatures was measured using a high-temperature rheometer (FRS1800, Anton Paar). The rheometer's spindle and

Table 1. Chemical compositions, measured viscosity at 1573 K, and liquidus and break temperature of the CA-based mold slag systems.

No.	SiO ₂ [wt%]	Al ₂ O ₃ [wt%]	CaO [wt%]	Na ₂ O [wt%]	Li ₂ O [wt%]	F [wt%]	B ₂ O ₃ [wt%]	SrO [wt%]	MgO [wt%]	K ₂ O [wt%]	TiO ₂ [wt%]	CaO/ Al ₂ O ₃	Al ₂ O ₃ / B ₂ O ₃	<i>T</i> _{liq} ^{a)} [K]	<i>T</i> _B ^{b)} [K]	<i>η</i> [Pa s]
0	1.0	34.8	38.3	8.0	6.0	1.0	10.0	0.0	0.0	1.0	0.0	1.10	3.50	1443		
1	1.0	38.3	38.3	8.0	6.0	1.0	6.5	0.0	0.0	1.0	0.0	1.00	5.90	1453	1448	0.37
2	1.0	39.3	38.3	8.0	6.0	1.0	5.5	0.0	0.0	1.0	0.0	1.00	7.20	1467	1440	0.43
3	1.0	40.3	38.3	8.0	6.0	1.0	4.5	0.0	0.0	1.0	0.0	0.90	9.00	1473	1438	0.52
													Li ₂ O/Na ₂ O			
4	1.0	39.3	38.3	9.0	5.0	1.0	5.5	0.0	0.0	1.0	0.0	1.00	0.60	1471		c)
5	1.0	39.3	38.3	10.0	4.0	1.0	5.5	0.0	0.0	1.0	0.0	1.00	0.40	1490		c)
6	1.0	39.3	38.3	10.9	3.0	1.0	5.5	0.0	0.0	1.0	0.0	1.00	0.30	1507		c)
7	1.0	39.3	38.3	11.9	2.0	1.0	5.5	0.0	0.0	1.0	0.0	1.00	0.20	1522		c)
8	1.0	39.3	38.3	12.9	1.0	1.0	5.5	0.0	0.0	1.0	0.0	1.00	0.10	1560		c)
9	7.3	30.9	35.5	10.6	2.4	3.7	0.0	0.0	1.7	2.1	5.8	1.10	0.23	1547	1524	0.353
10	7.2	30.5	33.7	10.5	2.4	3.6	0.0	2.6	1.7	2.1	5.7	1.10	0.23	1552	1521	0.411
11	7.1	30.1	31.7	10.3	2.4	3.6	0.0	5.5	1.7	2.1	5.6	1.10	0.23	1554		c)
12	7.1	29.7	29.7	10.2	2.3	3.5	0.0	8.3	1.6	2.0	5.5	1.00	0.23	1559		c)
13	7.4	31.3	31.8	10.7	2.5	3.7	0.0	0.0	4.7	2.1	5.8	1.00	0.23	1599		c)
14	6.9	28.9	37.1	9.9	2.3	6.1	0.0	0.0	1.6	2.0	5.4	1.28	0.23	1509	1486	0.283
15	6.4	27.1	38.4	9.3	2.1	8.2	0.0	0.0	1.5	1.9	5.1	1.42	0.23	1545		c)
16	5.9	25.0	40.1	8.6	2.0	10.7	0.0	0.0	1.4	1.7	4.7	1.60	0.23	1550		c)
17	6.9	29.1	37.3	10.0	1.6	6.1	0.0	0.0	1.6	2.0	5.4	1.28	0.16	1532	1529	0.368
18	7.0	29.3	37.6	10.0	1.0	6.1	0.0	0.0	1.6	2.0	5.5	1.28	0.10	1545	1538	0.407
19	7.0	29.4	37.8	10.1	0.3	6.2	0.0	0.0	1.6	2.0	5.5	1.28	0.03	1571	1553	0.428

^{a)}Liquidus temperature; ^{b)}Break temperature; ^{c)}Not measured.

cup were made from Pt90/Rh10 alloy with an inner cup diameter of 23 mm, and a spindle height and diameter of 25 and 19 mm, respectively, resulting in a measurement gap of 2 mm. For calibration at room temperature, standard oil S60, N100, and S200 (Cannon Instrument Company) was used. At high temperature, “Standard Glas 1” (Deutsche Glastechnische Gesellschaft e.V.) was utilized. A shear rate of 30 s⁻¹ was applied to the sample with a mass of 42 g. The pre-melted samples were heated within the rheometer to 1673 K and cooled at 5 K min⁻¹ until the maximum torque was reached. Gas purging was not performed. As the slags were found to damage the cup by volume expansion due to the changes in the minerals during cooling, only one measurement was performed for every sample. For some samples, the liquid slag foamed over the crucible; hence, there was no viscosity data obtained. For previous CS-based mold slags measurements, every run was repeated three times. The standard deviation of the viscosity for these mold fluxes at 1573 K was 0.006 Pa s, and that of the break temperature was 29 K.

3. Results and Discussion

3.1. Mold Flux Samples with B₂O₃

3.1.1. Compositions with Varying A/B Ratio

For all compositions of the first investigated series, B₂O₃ was replaced with the same amount (wt%) of Al₂O₃. As shown in

Table 1, a decrease in B₂O₃ and C/A ratio increases the viscosity of the sample, which correlates with the results of Kim and Sohn.^[21] The increase in the melting temperature was detected using DTA and FCT (see Figure 2a). The different temperatures obtained from these methods are attributed to their use of different heating rates and sample weights. Regarding the crystallization temperature (see Figure 2b), there is no particular trend observed. However, for FCT, the crystallization temperature increases with the increase in the Al₂O₃/B₂O₃ (A/B) ratio. A small peak, which is mainly attributed to the initial formation of lithium aluminate (LiAlO₂) at the Pt wire, is visible at ≈1490 K, whereas the main crystallization peak is observed at ≈1340 K. In contrast, the temperature of the first crystallization peak and the break temperature obtained with STA and rheometer, respectively, decrease with increasing A/B ratio, which can be attributed to the volatilization of LiF or BaBO₂.^[31] However, for this flux, the detected mass loss did not exceed 2.03 wt%. Unfortunately, due to the rheometer setup, it was not possible to recover the samples for chemical analysis after measurement without additional heat treatment. The quenched samples exhibit only minor crystallization at the surface. The crystalline fraction increases with increasing Al₂O₃ content, confirming that B₂O₃ has a positive effect on the glass-forming ability of the samples.^[27] The samples with lower B₂O₃ contents revealed higher viscosity. Nevertheless, this does not contribute to glass-forming tendency. LiAlO₂ is identified as the main phase in XRD analysis. Minor amounts of takedaite (Ca₃B₂O₆), Ca₃Al₂O₆, and lime

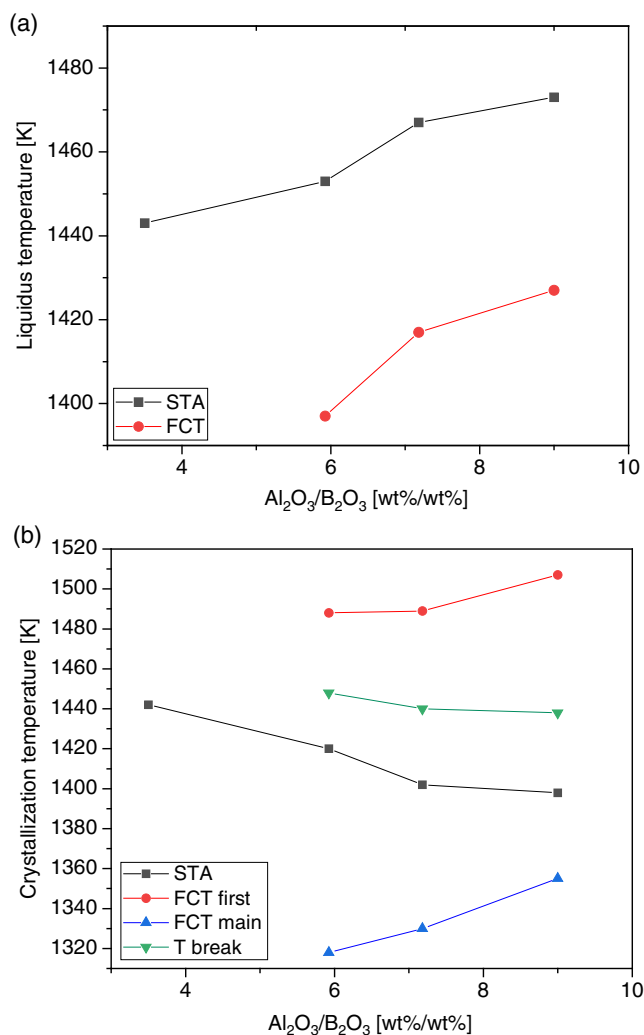


Figure 2. a) Liquidus and b) crystallization temperatures of the CA-based mold flux with varying A/B ratio.

(CaO) are also detected. After the FCT, the samples are noted to be fully crystallized, and Ca₃Al₂O₆ is identified as the primary phase. In addition to the aforementioned phases, sodium aluminum oxide (NaAlO₂) is also observed. As the A/B ratio increases, the amount of takedaite decreases, and that of Ca₃Al₂O₆ increases, whereas all other phases are not affected.

3.1.2. Compositions with Varying L/N Ratio

Based on sample 2, the amount of Li₂O (wt%) decreases by adding the same amount of Na₂O (wt%). Table 1 shows the significant increase in the liquidus temperature with the decrease in the LiO₂ content. The crystallization temperatures measured by STA for samples 4–8 are 1483, 1496, 1484, 1442, and 1488 K, respectively. Compared with sample 2, samples 4–8 have higher crystallization temperatures and are not affected by the Li₂O/Na₂O (L/N) ratio. Furthermore, the mass loss detected with STA did not exceed 2.03 wt%. As the melting temperature

showed an unfavorable increase, viscosity measurements were not performed. The calculations using the viscosity tool in FactSage indicate the increase in viscosity with decreasing L/N ratio. The operator observed the same trend during the quenching procedure when casting the liquid samples on the steel plate.

The changes in the composition of the samples have a significant effect on their glass-forming ability. Sample 2 (L/N = 0.8) solidified mainly glassy after the quench test. Through decreasing the L/N, the crystalline fraction increased until sample 8 (L/N = 0.1), in which no glassy phase was detected. The increase in viscosity does not hinder the sample from crystallizing. Microscopical investigations of the cross section using reflected light microscopy and SEM reveal the shift of the crystallization mechanism from surface to bulk nucleation. The phases formed in the quenched samples are LiAlO₂, NaAlO₂, Ca₃B₂O₆, Ca₃Al₂O₆, sodium calcium aluminate, and fluormayenite (Ca₆Al₇O₁₆F). By substituting Na₂O with Li₂O, the amount of LiAlO₂ increases, whereas those of sodium calcium aluminate and NaAlO₂ decrease. These findings are in line with those of Lu and co-workers,^[17] where the use of Li₂O instead of Na₂O was noted to be more effective in inhibiting crystallization. It should be noted that the different flux properties are not only caused by the different ion sizes of Na⁺ and Li⁺ but also by the lower molar weight of Li₂O, resulting in the decrease in the total number of network modifier R₂O molecules with the decrease in the L/N ratio.

3.2. Mold Flux Samples without B₂O₃

3.2.1. Compositions with the Substitution of CaO with SrO and MgO

The melting temperature significantly increases by more than 50 K (Table 1) for the sample without B₂O₃, compared with those with boron. Earth alkaline oxide BaO is known to inhibit crystallization^[32]; however, little is known about the use of SrO. Therefore, in this study, CaO was partly replaced with the same number of moles of SrO. Although crushed quenched samples were used for viscosity measurement, sample 11 overflowed from the rheometer, invalidating the results from this run. Therefore, for safety reasons, the measurement was not repeated, and viscosity measurements were only carried out for samples 9–11. Samples 9 and 10 proved that the addition of SrO increases the viscosity of the system, similar to BaO (Table 1). As shown in Table 1, the use of up to 8.3 wt% SrO increases the melting temperature by only 12 K from 1547 to 1559 K. The detected decrease in the break temperature by 3 K is considered insignificant, as it is within the standard deviation for this method. Furthermore, the restraining effect of BaO on the crystallization could not be achieved with SrO (Figure 3). The main crystalline phases, detected by XRD and SEM-EDS, are fluoromayenite, sodium calcium fluorosilicate (NaCa₂SiO₄F), villiamite (NaF), and cuspidine (Ca₄Si₂O₇F₂). Sr²⁺ and Ca²⁺ are interchangeable in a wide range of crystal structures.^[33,34] In the present study, the majority of Sr⁺ is realized with Na(Ca,Sr)₂SiO₄F; however, Sr is also detected with fluoromayenite and cuspidine. There is no additional SrO-containing phase formed within the investigated range. Therefore, the results demonstrate that the use of SrO

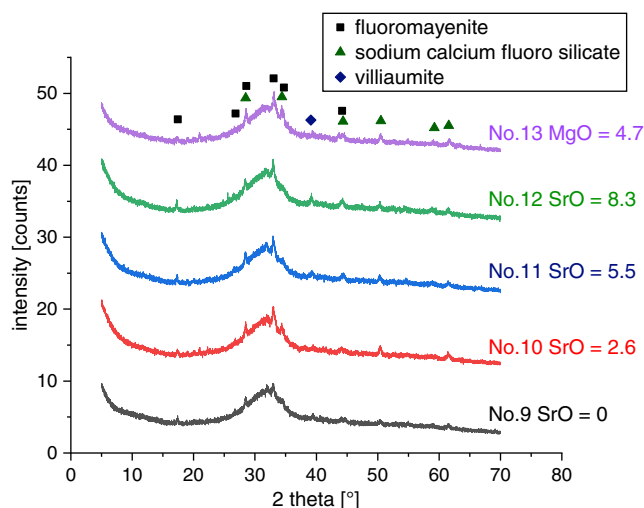


Figure 3. XRD patterns of the quenched samples, where CaO is substituted with SrO and MgO (wt%).

is not beneficial when adjusting the melting temperature, glass-forming ability, and viscosity of CA-based mold slags. Contrary to SrO, the increase in the MgO content from 1.7 to 4.7 wt% due to the equimolar replacement of CaO formed an additional high melting phase based on the STA results. In addition, the melting temperature increases from 1547 to 1599 K, exceeding the requirement for mold flux. Hence, there were no viscosity measurements performed for sample 13.

3.2.2. Compositions with Increasing CaF_2 Content

CaF_2 was added to the system to decrease the viscosity of sample 9. When the fluorine content increases from 3.7 to 6.1 wt%, the liquidus and break temperatures significantly decrease. Further increase in the fluorine content increases the melting temperature (Table 1). With rising fluorine content, a considerable increase in the mass loss during the heating and cooling cycles was observed with STA. The mass loss, which did not exceed 1.2 wt% until the melting temperature, started with the formation of a first liquid phase. The main volatilization occurred when the sample was completely liquid and ended when most of the sample solidified. The overall mass losses are 4.7, 5.3, 8.0, and 9.6 wt% for samples 9 and 14–16, respectively, which linearly correlate with the fluorine content of the samples. After the measurement of samples 15 and 16, slag droplets adhered to the lid of the crucible. This indicates that the results of these measurements are not reliable; thus, the crystallization temperature for these samples cannot be given. Moreover, because of the tendency of the samples to overflow from the crucible, no viscosity measurements were performed for samples 15 and 16 for safety reasons. The viscosity of sample 14 is less than that of sample 9, which has a lower fluorine content. This decline in viscosity through further CaF_2 addition from 6.9 wt% fluorine^[25] could not be reproduced due to the tendency of the samples to leak out of the crucible.

The increase in the fluorine content from 3.7 to 6.1 wt% (sample 14) did not affect the glass-forming ability of the sample

(Figure 4); the quenched samples obtained from both compositions were mainly glassy. Due to the complex role of F^- in the CA-based mold flux structure,^[9] the crystalline fraction rapidly increases, as the fluorine content increases to 8.2 wt% (sample 15). According to the XRD pattern, sample 16 (10.7 wt% fluorine) was nearly crystalline. With the increase in the fluorine content, the main phase changes from $\text{NaCa}_2\text{SiO}_4\text{F}$ to $\text{Ca}_6\text{Al}_7\text{O}_{16}\text{F}$. Moreover, small amounts of NaF are observed in the crystalline samples.

3.2.3. Compositions with Decreasing Li_2O Content

The effect of decreasing the Li_2O content on sample 14, which has the lowest liquidus temperature and viscosity, without the substitution of Na_2O was investigated. A decrease in the Li_2O content from 2.3 to 0.3 wt% linearly increases the liquidus temperature by 62 K (Table 1), thereby reducing the viscosity (Figure 5) and positively influencing the glass-forming ability of Li_2O .^[18] From the XRD pattern of the quenched samples, the crystalline fraction slightly increases with decreasing Li_2O content. In accordance with the liquidus temperature, the break temperature related to crystallization increases with decreasing Li_2O content. The viscosity curves indicate that more than one crystal phase precipitates from the liquid until the viscosity exceeds the maximum measurable value. The first crystalline phases formed in the quenched samples are $\text{Ca}_6\text{Al}_7\text{O}_{16}\text{F}$ and $\text{NaCa}_2\text{SiO}_4\text{F}$. The results of the samples quenched from 1673 to 1173 K and held for varying amounts of time, revealing that the samples are completely crystalline after 5 min, and their crystal phases further increase without changing their microstructure, as the dwelling is prolonged. In addition to $\text{Ca}_6\text{Al}_7\text{O}_{16}\text{F}$ and $\text{NaCa}_2\text{SiO}_4\text{F}$, Figure 6 shows the existence of sodium aluminum oxide ($(\text{Na,K})\text{AlO}_2$), NaF, and fluorite (CaF_2). With a decreasing Li_2O content, the amount of LiAlO_2 is reduced. Furthermore, the Li_2O content affects the formation of perovskite ($\text{Ca}(\text{Ti,Fe,Al,Si})\text{O}_3$) and $\text{NaCa}_2\text{SiO}_4\text{F}$, which is a solid solution that dissolves MgO and TiO_2 . With decreasing Li_2O content, the amount of TiO_2 dissolved in this phase increases, resulting in a considerable peak shift in the XRD pattern. In the samples with only 0.3 and 1.0 wt% Li_2O , götzenite ($\text{NaCa}_6\text{TiSi}_4\text{O}_{15}\text{F}_3$) is additionally formed. Meanwhile, in the samples with 1.6 and 2.3 wt% Li_2O , $\text{Ca}(\text{Ti,Fe,Al,Si})\text{O}_3$ is observed, and the amount of CaF_2 increases. In addition, the different Li_2O contents affect the crystal size of the sample. In particular, the largest crystals are formed in the slag with the highest Li_2O content, which can be attributed to the low viscosity of this mixture.

4. Conclusion

Although several reports on flux systems have been publicized in recent years, there is still limited data available on CA-based mold flux systems. Thus, this study investigated CA-based fluxes with a C/A ratio of 1 in terms of their liquidus temperature, crystallization behavior, and viscosity with respect to casting requirements. Therefore, two approaches were considered—compositions with and without B_2O_3 . Based on two starting compositions, the constituents were altered.

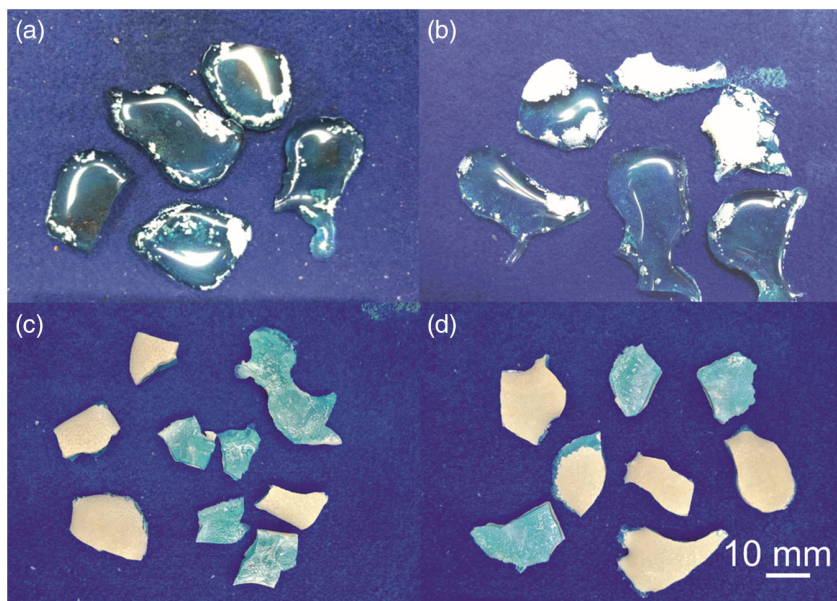


Figure 4. CA-based slags after quenching from 1673 K to room temperature with a) 7.46 wt% CaF₂, b) 12.48 wt% CaF₂, c) 16.99 wt% CaF₂, and d) 22.47 wt% CaF₂.

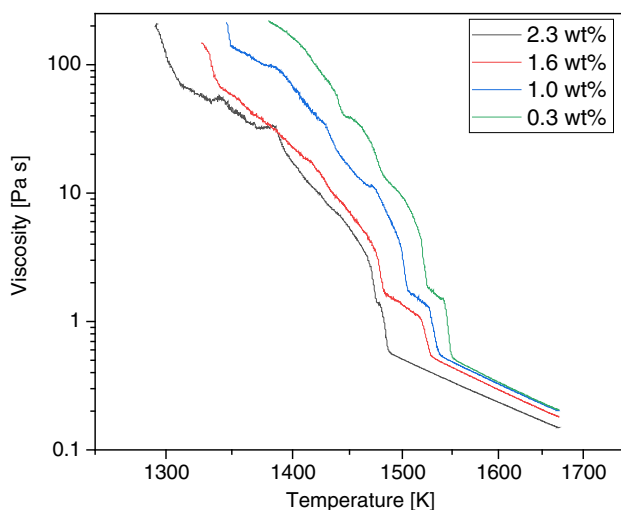


Figure 5. CA-based slag viscosity with varying Li₂O contents.

B₂O₃ lowers the liquidus temperature. For the B₂O₃ containing sample 1, a liquidus temperature of 1443 K and a viscosity at 1573 K of 0.37 Pa s are achieved with the A/B ratio of 5.9. Quenching results in amorphous samples. Increasing the A/B ratio from 5.9 to 9.0 leads to an increase in the liquidus temperature to 1473 K and a viscosity at 1573 K to 0.52 Pa s. The glass-forming ability is reduced. The first precipitating phase is LiAlO₂, whereas the primary phase is Ca₃Al₂O₆ in the fully crystallized sample.

Li₂O effectively decreases the liquidus temperature and viscosity and enhances the glass-forming ability. A decrease in the L/N ratio of sample 2 (A/B ratio of 5.9) from 0.8 to 0.1 increases the liquidus temperature from 1493 to 1560 K. The main phase alters

from LiAlO₂ to sodium calcium aluminate and NaAlO₂. Lowering the L/N ratio of B₂O₃-free sample 14 from 0.23 to 0.03 increases the liquidus temperature from 1509 to 1571 K and the viscosity at 1573 K from 0.283 to 0.428 Pa s. Instead of the main phase NaCa₂SiO₄F, the mineral phase Ca₆Al₇O₁₆F crystallizes. For samples with and without boron, the crystalline fraction is increased with decreasing Li₂O content.

The substitution of CaO for 8.3 wt% SrO in the B₂O₃-free composition (sample 9) results in a slight increase in the liquidus temperature from 1547 to 1559 K. With 2.6 wt% SrO, the viscosity at 1573 K increased from 0.35 to 0.41 Pa·s. The good glass-forming ability is not altered. After quenching, the main crystalline phases are (Ca,Sr)₆Al₇O₁₆F and Na(Ca,Sr)₂SiO₄F. Thus, a low amount of SrO is not beneficial in adjusting the melting temperature, glass-forming ability, and viscosity of the CA-based mold flux.

Contrary to CS-based fluxes, for the boron-free slag (sample 9), a fluorine content of only up to 6.1 wt% decreases the liquidus temperature to 1509 K and a viscosity at 1573 K to 0.283 Pa s. Further addition of fluorine to 10.7 wt% increases the liquidus temperature (to 1550 K), crystallization, and mass loss in the liquid state. The main phase changes from NaCa₂SiO₄F to Ca₆Al₇O₁₆F.

In general, lower viscosity promotes diffusion processes. In this work, the increase in the crystallization temperature overruled the viscosity and increased the overall crystallinity of the quenched samples.

In particular, sample 1 (6.5 wt% B₂O₃ and 6 wt% Li₂O) and sample 14 (0 wt% B₂O₃, 2.3 wt% Li₂O, and 6.1 wt% F) exhibit the best results in terms of the liquidus temperature and viscosity. In addition, they show glass-forming tendency during quenching. Thus, both may be regarded to be used in the continuous casting process. Nevertheless, the effect of the evaporation should be evaluated further.

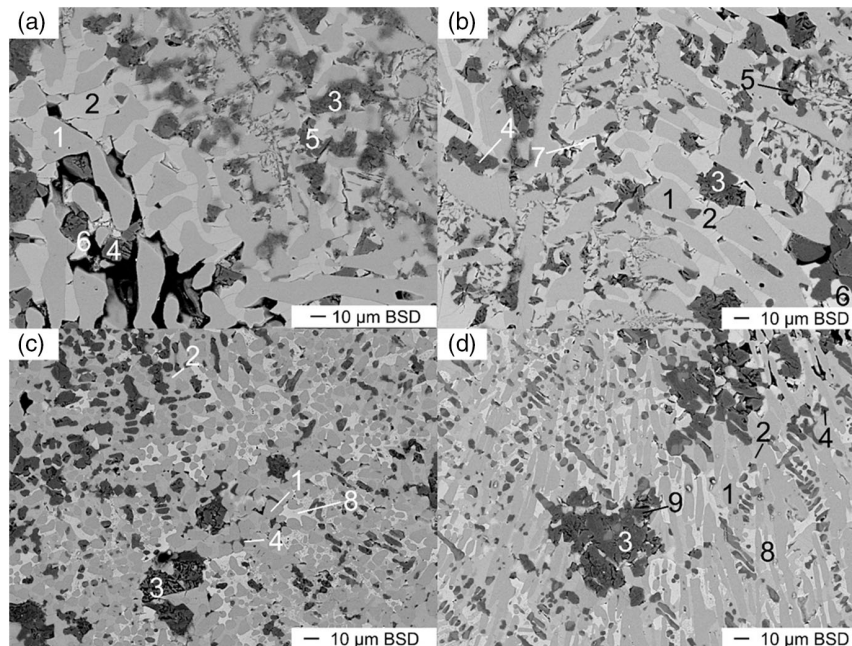


Figure 6. Microstructure of the CA-based slags after quenching from 1673 to 1173 K for 15 min: a) 2.3 wt% Li₂O, b) 1.6 wt% Li₂O, c) 1.0 wt% Li₂O, and d) 0.3 wt% Li₂O; 1) Ca₁₂Al₁₄O₃₂F₂, 2) NaCa₂SiO₄F, 3) (Na,K)AlO₂, 4) NaF, 5) LiAlO₂, 6) CaF₂, 7) Ca(Ti,Fe,Al,Si)O₃, 8) NaCa₆TiSi₄O₁₅F₃, and 9) MgO.

Acknowledgements

The authors gratefully acknowledge the funding support of K1-MET GmbH, a metallurgical competence center. The research program of the K1-MET competence center is supported by Competence Center for Excellent Technologies (COMET), the Austrian program for competence centers. COMET is funded by the Federal Ministry for Climate Action, Environment, Energy, Mobility, Innovation and Technology, the Federal Ministry for Digital and Economic Affairs, the Federal States of Upper Austria, Tyrol, and Styria as well as the Styrian Business Promotion Agency (SFG). Furthermore, thank goes to Upper Austrian Research GmbH for their continuous support. In addition to public funding from COMET, partial financing comes from the industrial partners RHI Magnesita, voestalpine Stahl, and voestalpine Stahl Donawitz and the scientific partner Montanuniversität Leoben.

Conflict of Interest

The authors declare no conflict of interest.

Data Availability Statement

Data available on request due to privacy/ethical restrictions.

Keywords

calcium–aluminate-based mold flux, liquidus temperature, mineralogical composition, viscosity

Received: March 29, 2021
Revised: May 11, 2021
Published online: June 9, 2021

- [1] K. C. Mills, *ISIJ Int.* **2016**, *56*, 14.
- [2] I. Marschall, N. Kölbl, H. Harmuth, G. Xia, *J. Manuf. Sci. Prod.* **2013**, *13*, 103.
- [3] P. Ni, T. Tanaka, M. Suzuki, M. Nakamoto, M. Ersson, P. G. Jönsson, *ISIJ Int.* **2019**, *59*, 2024.
- [4] H. Cui, K. Zhang, Z. Wang, B. Chen, B. Liu, J. Qing, Z. Li, *Metals* **2019**, *9*, 204.
- [5] W. Yan, Y. D. Yang, W. Q. Chen, M. Barati, A. McLean, *Can. Metall. Q.* **2015**, *54*, 467.
- [6] J.-W. Cho, K. Blazek, M. Frazee, H. Yin, J. H. Park, S.-W. Moon, *ISIJ Int.* **2013**, *53*, 62.
- [7] Q. Shu, J. L. Klug, Q. Li, *ISIJ Int.* **2019**, *59*, 1057.
- [8] Q. Liu, G. Wen, J. Li, X. Fu, P. Tang, W. Li, *Ironmaking Steelmaking* **2014**, *41*, 292.
- [9] J. Gao, G. Wen, T. Huang, B. Bai, P. Tang, Q. Liu, *J. Am. Ceram. Soc.* **2016**, *99*, 3941.
- [10] L. Zhou, H. Li, W. Wang, Z. Wu, J. Yu, S. Xie, *Metall. Mater. Trans. B* **2017**, *48*, 2949.
- [11] M. Leng, F. Lai, J. Li, *Materials* **2018**, *12*, 62.
- [12] X. J. Fu, G. H. Wen, P. Tang, Q. Liu, Z. Y. Zhou, *Ironmaking Steelmaking* **2014**, *41*, 342.
- [13] W. Wang, B. Lu, D. Xiao, *Metall. Mater. Trans. B* **2016**, *46*, 384.
- [14] J. Qi, C. Liu, M. Jiang, *Can. Metall. Q.* **2017**, *56*, 212.
- [15] J. L. Li, Q. F. Shu, K. C. Chou, *Can. Metall. Q.* **2015**, *54*, 85.
- [16] E. Gao, W. Wang, L. Zhang, *J. Non-Cryst. Solids* **2017**, *473*, 79.
- [17] T. Wu, Q. Wang, S. He, J. Xu, X. Long, Y. Lu, *Steel Res. Int.* **2012**, *83*, 1194.
- [18] B. Lu, K. Chen, W. Wang, B. Jiang, *Metall. Mater. Trans. B* **2014**, *45*, 1496.
- [19] D. Janke, P. Hammerschmid, Stollberg GmbH, Max-Planck-Institut für Eisenforschung, US 5782956A, **1998**.
- [20] L. Chen, K. Liu, P. Han, B. Yang, L. Feng, *J. Chem.* **2020**, *2020*, 1.
- [21] G. H. Kim, I. Sohn, *Metall. Mater. Trans. B* **2014**, *45*, 86.
- [22] W. Yan, W. Chen, Y. Yang, C. Lippold, A. McLean, *Ironmaking Steelmaking* **2016**, *43*, 316.
- [23] L. Zhang, W. Wang, H. Shao, *J. Iron Steel Res. Int.* **2019**, *26*, 336.

- [24] W. Yan, W. Chen, Y. Yang, A. McLean, *Ironmaking Steelmaking* **2019**, 46, 347.
- [25] D.-L. Zheng, J. Li, C.-B. Shi, J.-T. Ju, *Ironmaking Steelmaking* **2018**, 45, 135.
- [26] C.-B. Shi, M.-D. Seo, J.-W. Cho, S.-H. Kim, *Metall. Mater. Trans. B* **2014**, 45, 1081.
- [27] J. Yang, J. Zhang, O. Ostrovski, C. Zhang, D. Cai, *Metall. Mater. Trans. B* **2019**, 50, 291.
- [28] S. S. Jung, I. Sohn, *Metall. Mater. Trans. B* **2012**, 43, 1530.
- [29] T. Wu, S.-P. He, Y.-T. Guo, Q. Wang, in *Characterization of Minerals, Metals, and Materials*, Vol. 5 (Eds: J. S. Carpenter, C. Bai, J.-Y. Hwang, S. Ikhmayies, B. Li, S. N. Monteiro, Z. Peng, M. Zhang), John Wiley & Sons, Inc, Hoboken, NJ **2014**, pp. 265.
- [30] Y.-R. Cui, H.-Y. Fan, Z.-L. Guo, G.-H. Wang, X.-M. Li, J.-X. Zhao, Z. Yang, *J. Iron Steel Res. Int.* **2019**, 26, 412.
- [31] L. Wang, J. Zhang, Y. Sasaki, O. Ostrovski, C. Zhang, D. Cai, *Metall. Mater. Trans. B* **2017**, 48, 1055.
- [32] D. Xiao, W. Wang, B. Lu, *Metall. Mater. Trans. B* **2015**, 46, 873.
- [33] M. Ceh, D. Kolar, L. Golic, *J. Solid State Chem.* **1987**, 68, 68.
- [34] E. Renaud, C. Robeline, M. Heyrman, P. Chartrand, *J. Chem. Thermodyn.* **2009**, 41, 666